JOURNAL OF GEOPHYSICAL RESEARCH, VOL. 113, C02002, doi:10.1029/2006JC003994, 2008

Click Here for Full Article

Physical mechanisms for the offshore detachment of the Changjiang Diluted Water in the East China Sea

Changsheng Chen,[1,2] Pengfei Xue,[1] Pingxing Ding,[2] R. C. Beardsley,[3] Qichun Xu,[1] Xianmou Mao,[4] Guoping Gao,[1,5] Jiahua Qi,[1] Chunyan Li,[6] Huichan Lin,[7] Geoffrey Cowles,[1] and Maochong Shi[5]

Received 27 October 2006; revised 2 April 2007; accepted 8 August 2007; published 2 February 2008.

[1] Physical mechanisms for the summertime offshore detachment of the Changjiang Diluted Water (CDW) into the East China Sea are examined using the high-resolution, unstructured-grid, Finite-Volume Coastal Ocean Model (FVCOM). The model results suggest that isolated low salinity water lens detected west of Cheju Island can be formed by (1) a large-scale adjustment of the flow field to the Changjiang discharge and (2) the detachment of anticyclonic eddies as a result of baroclinic instability of the CDW front. Adding the Changjiang discharge intensifies the clockwise vorticity of the subsurface current (originating from the Taiwan Warm Current) flowing along the 50-m isobath and thus drives the low-salinity water in the northern coastal area of the Changjiang mouth offshore over a submerged plateau that extends toward Cheju Island. Given a model horizontal resolution of less than 1.0 km, the CDW front becomes baroclinically unstable and forms a chain of anticyclonic and cyclonic eddies. The offshore detachment of anticyclonic eddies can carry the CDW offshore. This process is enhanced under northward winds as a result of the spatially nonuniform interaction of wind-induced Ekman flow and eddy-generated frontal density currents. Characteristics of the model-predicted eddy field are consistent with previous theoretical studies of baroclinic instability of buoyancy-driven coastal density currents and existing satellite imagery. The plume stability is controlled by the horizontal Ekman number. In the Changjiang, this number is much smaller than the criterion suggested by a theoretical analysis.

Citation: Chen, C., et al. (2008), Physical mechanisms for the offshore detachment of the Changjiang Diluted Water in the East China Sea, *J. Geophys. Res.*, *113*, C02002, doi:10.1029/2006JC003994.

1. Introduction

[2] In 1986, an international collaboration among American, Chinese, and Korean scientists made two regional hydrographic surveys in the East China/Yellow Seas (Figure 1) during 8 January to 1 February and 4–20 July [*Chen et al.*, 1994]. The summer survey clearly showed an isolated low-salinity lens in the region near 32.5°N, 124°E between the Changjiang and Cheju Island (Figure 2). This unique summertime distribution of salinity was detected in earlier field measurements off the Changjiang [*Beardsley et al.*, 1985] and recent field data collected east of Cheju Island [*Lie et al.*, 2003]. It is commonly thought that the low-salinity water lens originates from the Changjiang Diluted Water (CDW). During the summer high river discharge season, this water can be detached eastward from the Changjiang plume as a result of either vortex stretching [*Beardsley et al.*, 1985] or summer monsoon-driven offshore advection [*Isobe et al.*, 2002; *Chang and Isobe*, 2003].

[3] The eastward movement of CDW was also suggested in the tracks of two surface drifters deployed in July 1986 [*Beardsley et al.*, 1992]. Drifter 6986, which was launched with a drogue at 10 m below the surface in the CDW plume northeast to the mouth of the Changjiang, rotated anticyclonically at a mean speed of 13 cm/s in the first 2 weeks and then moved quickly toward Cheju Island at a speed of 14–20 cm/s (Figure 3). This drifter flowed through Cheju Strait and eventually entered the Japan/East Sea (JES) through the western channel of the Tsushima/Korea Strait. The eastward flow in Cheju Strait was also evident in the

[1]Department of Fisheries Oceanography, Intercampus Graduate School for Marine Science and Technology, University of Massachusetts, New Bedford, Massachusetts, USA.
[2]State Key Laboratory for Estuarine and Coastal Research, East China Normal University, Shanghai, China.
[3]Department of Physical Oceanography, Woods Hole Oceanographic Institution, Woods Hole, Massachusetts, USA.
[4]State Key Laboratory of Satellite Ocean Environment Dynamics, Second Institution of Oceanography, State Oceanic Administration, Hangzhou, China.
[5]College of Physical and Environmental Oceanography, Ocean University of China, Qingdao, China.
[6]Department of Oceanography and Coastal Sciences, School of the Coast and Environment, Louisiana State University, Baton Rouge, Louisiana, USA.
[7]Marine Extension Service, University of Georgia, Athens, Georgia, USA.

Copyright 2008 by the American Geophysical Union.
0148-0227/08/2006JC003994$09.00

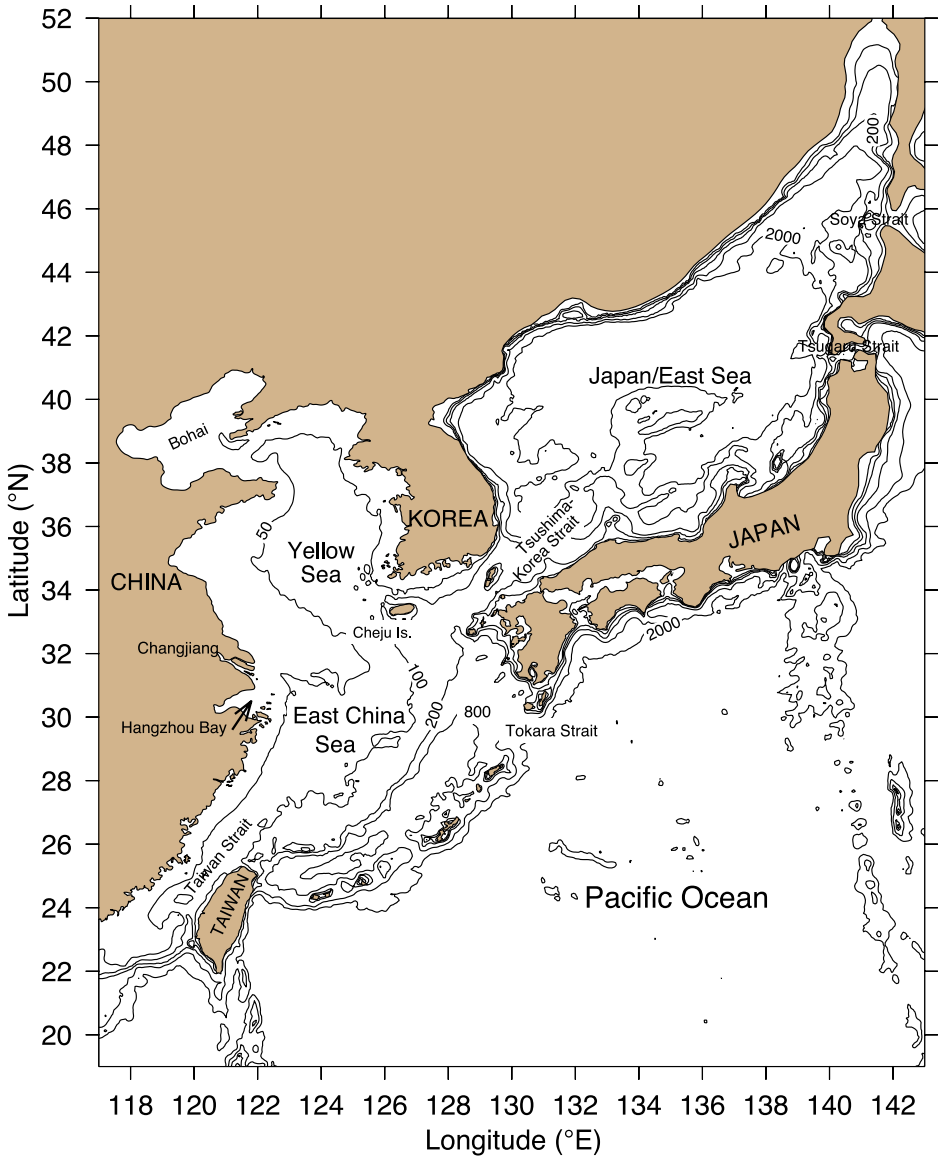

Figure 1. Bathymetry (in meters) and locations of the East China Sea, the Yellow Sea, the Bohai Sea, and the Japan/East Sea.

trajectory of drifter 6988 deployed with a drogue at 10 m below the surface west of Cheju Island in July (Figure 3). That drifter moved eastward at a speed of about 20–28 cm/s through Cheju Strait and then entered Tsushima/Korea Strait.

[4] The past and recent hydrographic and drifter measurements raise a fundamental question regarding the physical mechanisms for the formation of the isolated low-salinity lens west of Cheju Island. It is clear that CDW can be advected eastward by the southerly dominated summer monsoon wind but unclear how the wind interacts with the buoyant CDW plume to cause the offshore detachment of CDW in a large shallow region bounded by 50-m isobath between the Changjiang mouth and Cheju Island. Can CDW detach from the main body of the plume without wind forcing? If so, what other process is important?

[5] To address these questions, we must resolve the spatial/temporal structure of the Changjiang plume in the East China Sea (ECS). The Changjiang river mouth has complex coastal geometry and abruptly varying bathymetry (Figure 4). It is divided into southern and northern branches by Chongming Island. Two smaller islands are located in the mouth of the southern branch, which divides this branch into two channels. At the mouth of the river, the bottom topography features four "deep" passages connected to the southern branch. There are also two relatively deep passages linked to the northern branch. In the summer flood season, the Changjiang freshwater water splits into two streams at the northern tip of Chongming Island which flow out onto the inner shelf of the ECS through southern and northern branches [*Kong et al.*, 2004]. In the winter dry season, the Changjiang freshwater water flows into the ECS primarily through the southern branch and a saltwater return flow is frequently observed in the northern branch [*He et al.*, 2006]. In view of the plume dynamics, the Changjiang discharge is like a multiple river/estuarine system in which the offshore

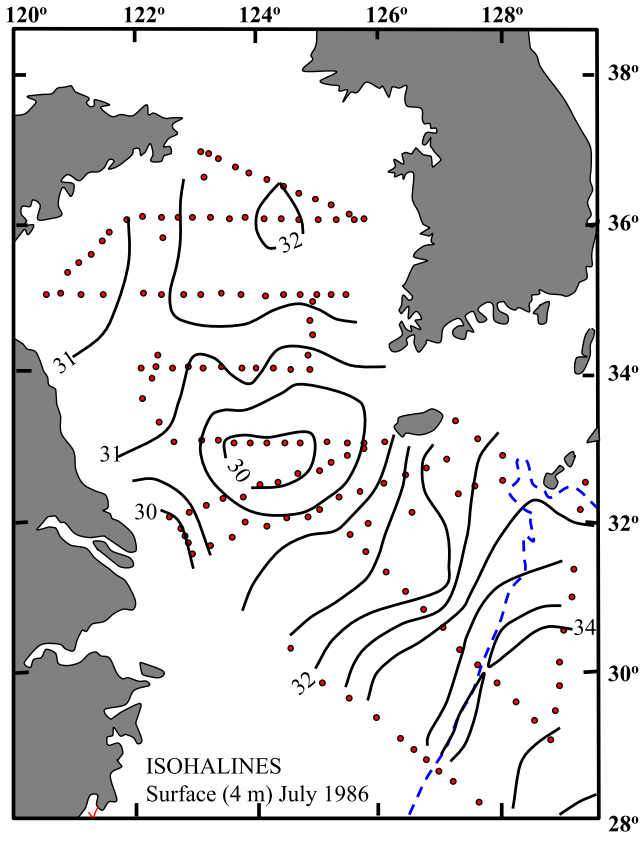

Figure 2. The distribution of salinity at a depth of 4 m below the surface measured on a large-scale survey in July 1986. The dots are the locations of the CTD stations and dashed line is the 200-m isobath. This figure was digitized from *Chen et al.* [1994].

detachment of plume water may be caused by eddy formation due to baroclinic instability of the plume [*Qiu et al.*, 1988] or by nonlinear interaction between upwelling-favorable wind and buoyancy flow at the low-salinity front [*Chen et al.*, 1999; *Chen*, 2000].

[6] A few modeling studies have explored the offshore eastward transport of CDW in the ECS [e.g., *Isobe et al.*, 2002; *Chang and Isobe*, 2003]. These models captured wind-driven eastward transport in the ECS, but realistic plume dynamics were restricted due to difficulties in resolving the complex bathymetry of the Changjiang rive mouth region. In previous structured-grid, finite-difference models of the ECS, the Changjiang discharges were either specified as a point source or an idealized short channel flow. Ignoring the actual along-river surface pressure gradient in the Changjiang can cause an overestimation of the offshore advection and failure to resolve the nature of multiple outflows. The horizontal resolution used in these models was too coarse to resolve the abruptly varying bottom topography in the river channels and thus the models were unable to simulate the mesoscale structure of the Changjiang plume over the inner shelf of the ECS. As a result, the buoyancy contribution to the water transport, particularly for the offshore eastward detachment of CDW, was significantly underestimated.

[7] A research team from the University of Massachusetts-Dartmouth (UMASS-D), East China Normal University (ECNU), and Woods Hole Oceanographic Institution (WHOI) led by C. Chen (UMASS-D), P. Ding (ECNU), and R. C. Beardsley (WHOI) have applied the unstructured-grid, Finite-Volume Coastal Ocean Model (FVCOM) to study the physical mechanisms for the offshore detachment of CDW in the ECS. FVCOM was originally developed by *Chen et al.* [2003] and improved by a team of UMASS-D and WHOI researchers [*Chen et al.*, 2004, 2006a, 2006b]. The unstructured triangular grid used in FVCOM allows us to

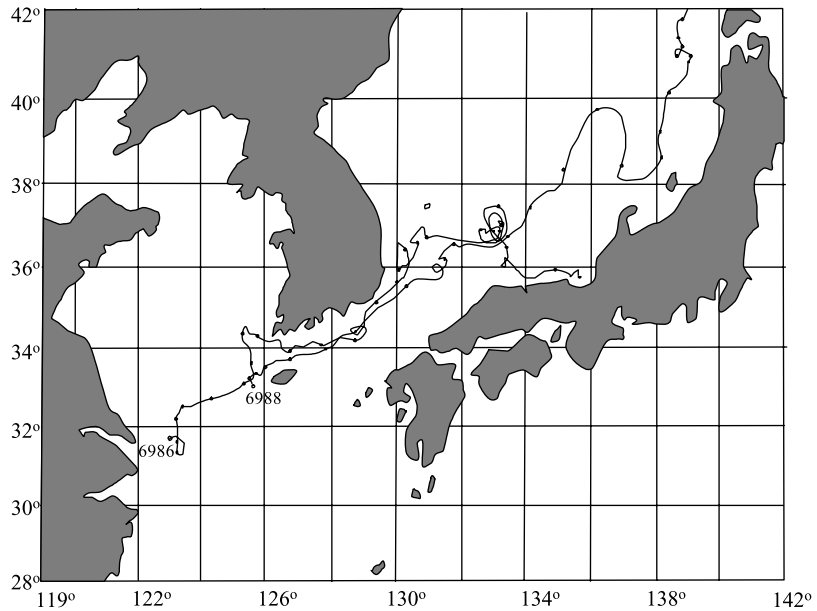

Figure 3. Trajectories of drifters 6986 and 6988 with drogues at 5 m below the surface. The drifters were released in summer 1986. Dots indicate the drifter locations every 5 d from launch. The data used in this figure were digitized from *Beardsley et al.* [1992, Figure 4].

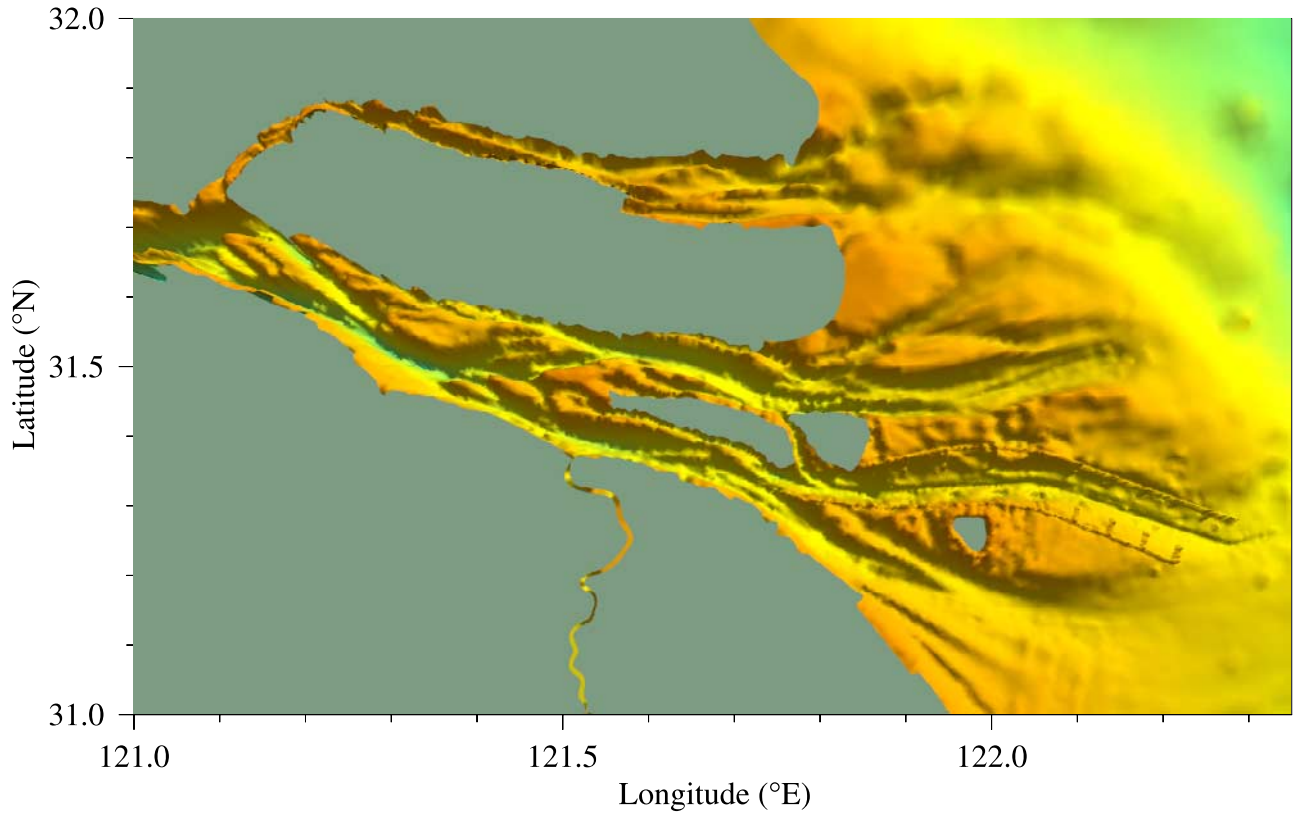

Figure 4. Three-dimensional bathymetry of the Changjiang and its adjacent shelf region.

include realistic coastline and bathymetry of the Changjiang and place higher horizontal resolution in the plume area. The finite-volume approach used in FVCOM guarantees local mass, momentum, heat, and tracer conservation, making it possible to trace the spread of CDW during a long-term integration.

[8] This paper describes the initial development of the ECS-FVCOM model system and its application to examine the role of the Changjiang discharge in the summertime adjustment of the ECS circulation and the contribution of plume instability to the offshore detachment of CDW. A series of idealized process-oriented numerical experiments were conducted and the model results compared with buoyant plume theory and remote-sensing data to develop physical insight into the low-salinity plume dynamics in the ECS.

[9] The remaining part of this paper is organized as follows. ECS-FVCOM and the design of numerical experiments are described in section 2. The process-oriented numerical model results under different physical conditions are presented in section 3. Section 4 presents a discussion and the conclusions summarized in section 5.

2. ECS-FVCOM and Design of Numerical Experiments

[10] ECS-FVCOM is a spherical coordinate version of the unstructured-grid finite-volume, three-dimensional (3-D) primitive equation coastal ocean model developed originally by *Chen et al.* [2003] and upgraded by the UMASS-D/WHOI model development team [*Chen et al.* 2006a, 2006c]. In common with other free-surface coastal models, FVCOM uses the modified Mellor and Yamada level 2.5 (MY-2.5) and Smagorinsky turbulent closure schemes as default setups for vertical and horizontal mixing, respectively [*Mellor and Yamada*, 1982; *Galperin et al.*, 1988; *Smagorinsky*, 1963]. Similar to popular structured-grid models like the Princeton Ocean Model (POM) and Regional Ocean Model system (ROMs), FVCOM is numerically solved using a split-mode method. The external mode is composed of vertically integrated transport equations in which the water elevation is solved explicitly using a shorter time step constrained by the ratio of the horizontal resolution to the phase speed of the long surface gravity wave. The internal mode consists of fully 3-D governing equations and is solved using a longer time step constrained by the phase speed of the lowest mode internal wave. Linkage between external and internal modes is through the water elevation, with mode adjustments based on the vertically integrated volume transport at each internal time step. Unlike structured-grid finite-difference and unstructured-grid finite-element models, FVCOM solves the flux form of the governing equations in unstructured triangular volumes by a second-order accurate discrete flux scheme. The finite-volume approach used in FVCOM takes advantage of finite-element methods in geometric flexibility and finite-difference methods in computational efficiency and provides an accurate representation of mass, momentum, heat, and salt conservation. (See http://fvcom.smast.umassd.edu/ for a full description of FVCOM, recent additions to its capabilities, and related publications.)

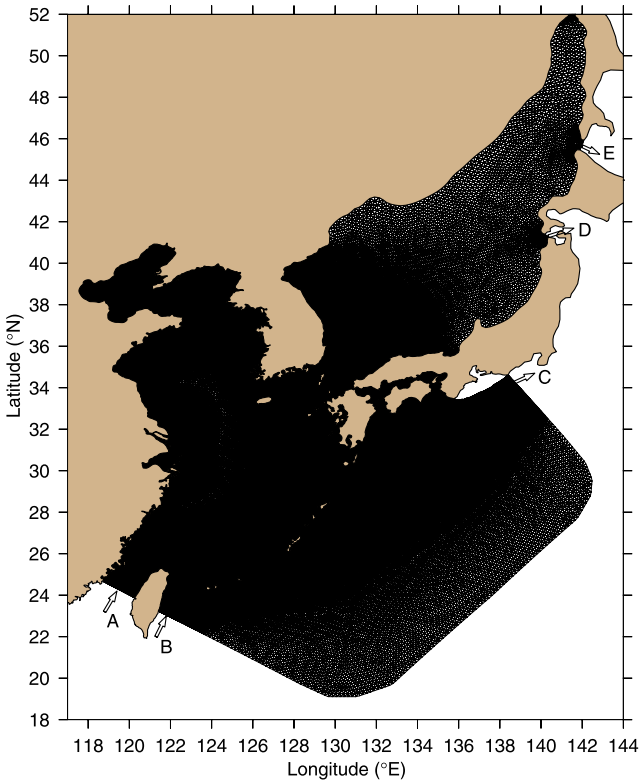

Figure 5. Unstructured grid of the East China Sea FVCOM. Labels A, B, C, D, and E indicate sections of the open boundary where water transports were specified.

[11] The computational domain of ECS-FVCOM covers the entire ECS, Yellow Sea (YS), Bohai Sea (BS), and Japan/East Sea (JES) (Figure 5). The domain is bounded by four open boundaries: Taiwan Strait (A), a line starting at the eastern coast of Taiwan (B), running off the slope of the ECS and then crossing onto the eastern shelf of Japan (C), Tsugaru Strait (D), and Soya Strait (E). The unstructured triangular grid has a horizontal resolution varying from 0.1 to 0.5 km in the Changjiang, 0.5–1.5 km in the river mouth area and along the coast, ~3-km in the path of the Kuroshio, and ~10–15 km in the interior of the ECS/YS/BS/JES and Pacific Ocean. An enlarged view of the triangular grid in the Changjiang area is shown in Figure 6. In the vertical, the domain is divided into 30 uniform σ-layers, which corresponded to a vertical resolution of 1.7 m or less in the Changjiang and coastal region where the water depth is shallower than 50 m. To reduce the model spin-up time, the model bathymetry off the slope in the western Pacific Ocean is cut at 800 m, a roughly e-folding depth of the Kuroshio Current.

[12] In this study, ECS-FVCOM is forced by (1) the Changjiang freshwater discharge at the upstream end of the Changjiang model domain and (2) a constant uniform wind stress. The model is initialized using 10-km resolution 3-D August climatology hydrographic fields and a specified water transport of the Kuroshio at the open boundary. The hydrographic fields were constructed using 10-km box averaging of historical water temperature and salinity data collected in this region over the last 40 a. The inflow transports are (1) 2.1 Sv for the Taiwan Warm Current (TWC) through A and (2) 27.5 Sv for the Kuroshio east of Taiwan through B. These are balanced by outflow transports of (1) 26.9 Sv for the Kuroshio southeast of Japan (C), (2) 1.6 Sv through the Tsugaru Strait (D), and (3) 1.1 Sv through the Soya Strait (E). The outflow transport on C was adjusted to balance an additional inflow from the Changjiiang when the river discharge was added. The inflow and outflow transport values used here are based on the summertime climatology conditions. The Kuroshio transport was estimated from current profiles in the upper 800 m, which is 1.0–2.0 Sv smaller than the total Kuroshio transport. Vertical profiles of the inflow and outflow Kuroshio transports are specified based on the observed structure of the Kuroshio from our previous ADCP measurements [*Chen et al.* 1992].

[13] Numerical experiments were conducted in three steps: day 0–30 spin-up with the climatology fields; day 31–60 spin-up with the Changjiang discharge; and day 61–90 run with (1) river discharge only (case A) and (2) river discharge and wind (case B). In particular, the model was first spun up with the August climatology hydrographic fields and fixed inflow and outflow transports for 60 model days. Since the Kuroshio and shelf circulation reached quasi-steady state after 30 model days, the river discharge was started on model day 31 by adding a freshwater discharge of 60,000 m^3/s (a typical summertime value) at the upstream end grid of the Changjiang domain. The Changjiang plume was established by model day 60. For the river discharge only case A, the model was run for an additional 30 d. For case B with river and wind forcing, the

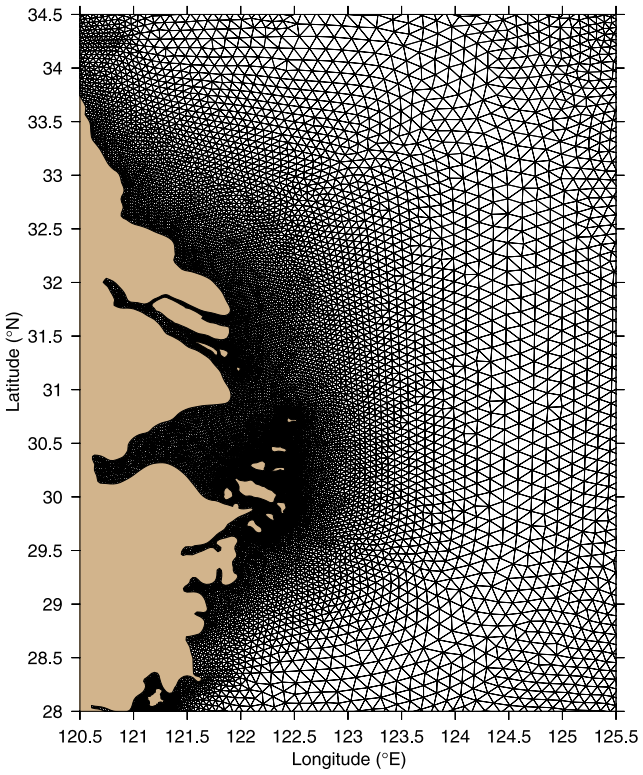

Figure 6. An enlarged view of the unstructured grid in the Changjiang area.

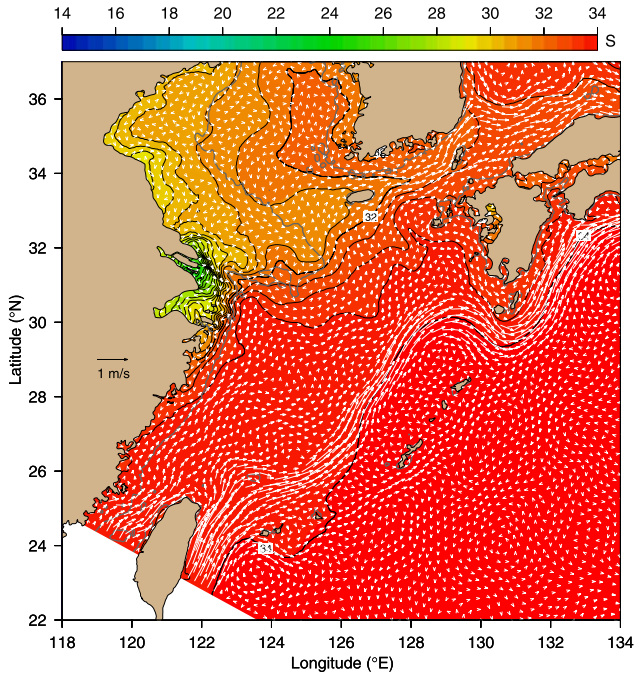

Figure 7. Distribution of near-surface current and salinity in the East China Sea on day 30 for the model run started with August climatology temperature and salinity fields. To make the vector fields more viewable, current vectors were selected in a search radius of ~20 km.

model was run for an additional 30 d followed by 7 d with no wind (to simulate a wind relaxation).

3. Model Results

3.1. Adjustment of the ECS Circulation to the Changjiang Discharge

[14] By model day 30, the Kuroshio and ECS, YS, BS, and JES circulation reach a quasi-steady state (Figure 7). The Kuroshio, with a mean velocity of ~100 cm/s, forms over the continental slope, entering the ECS east of Taiwan, flows along the 200-m isobath on the slope of the ECS, turns southeastward to go through the Tokara Strait and then moves northeastward along the Japanese coast to leave the computational domain. The TWC flows northeastward parallel to the 50-m isobath, enters a submerged river valley off the Changjiang and then turns anticyclonically along the 50-isobath to move onto the interior of the ECS continental shelf. The Yellow Sea Coastal Current (YSCC), Yellow Sea Warm Current (YSWC), Tsushima Warm Current, and Korean Coastal Current (KCC) are all resolved in this climatology-based flow field. The simulated circulation patterns agree well with previous field measurements summarized by *Qiu and Imasato* [1990], *Lie et al.* [1998], and *Ichikawa and Beardsley* [2002].

[15] The addition of the Changjiang discharge changes the circulation pattern in the shelf region between the river mouth and the Tsushima/Korea Strait (Figure 8). CDW flows out from the Changjiang from both southern and northern branchs, turning anticyclonically in the river mouth area shallower than 50 m before flowing southward along the coast. Correspondingly, the TWC, YSCC, YSWC, and Tsushima Warm Current are all intensified, even though the path and intensity of the Kuroshio change little. As a result, the northward transport of saline water is enhanced in the submerged river valley off the Changjiang and west of Cheju Island, and in turn a large portion of the low-salinity water (~30–32 PSU) is advected onto the shallow plateau bounded by the 50-m isobath by the enhanced YSCC and flows through the Cheju Strait and then Tsushima/Korea Strait as part of an intensified Tsushima Current. The local adjustment of the circulation off the Changjiang can be viewed more clearly in Figure 9, which shows that the less saline water patch detected over the submerged plateau between the Changjiang and Cheju Island can be advected from the western coast of the YS as a result of the current adjustment to the Changjiang discharge.

[16] The intensification of the TWC is evident in a comparison of the flow field at a depth of 20 m below the surface between the cases without and with the Changjiang discharge (Figure 10). With no river outflow, the relatively weak northward subsurface current has a magnitude of about 3–5 cm/s in and around the submerged river valley. After the CDW plume forms in the upper water layer, the northward current at the depth of 20 m is significantly larger (~10 cm/s or larger) and drives a relatively strong offshore flow along the 50-m isobath near the tip of this valley. This subsurface offshore flow can act like an "interior stress" to push the near-surface less-saline water eastward onto the plateau area east of the submerge valley.

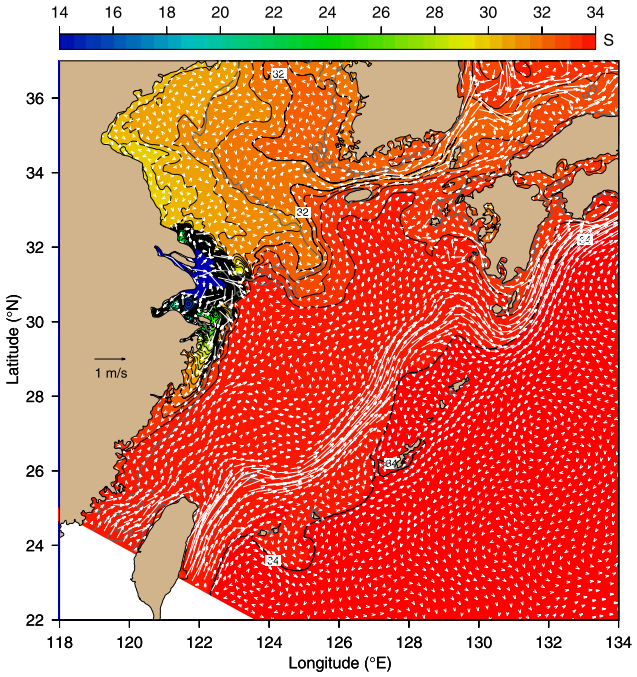

Figure 8. Distribution of near-surface current and salinity in the East China Sea and Changjiang estuary on day 30 after the Changjiang discharge was added. The river discharge was specified as a constant 60,000 m^3/s and added into the model after the current field (with the climatology hydrography) reached a quasi-steady state (Figure 7). The current vectors were selected in a search radius of ~20 km.

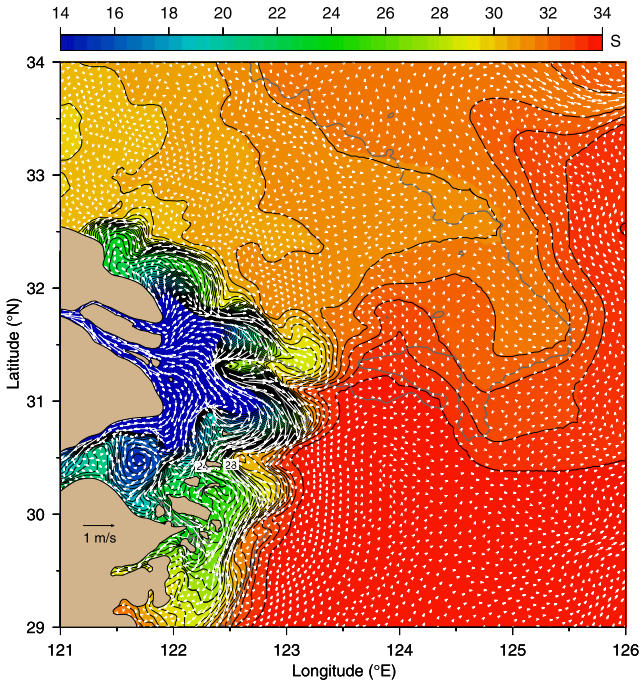

Figure 9. An enlarged view of the near-surface CDW plume current and salinity off the Changjiang at the same time as that in Figure 8. The current vectors drawn in this figure were selected in a search radius of ~5 km.

[17] This simple adjustment experiment suggests that the summertime circulation in the ECS and YS as well as in the Tsushima/Korea Strait is significantly influenced by the Changjiang discharge. The summertime intensification of the TWC, YSWC, YSCC, and Tsushima Warm Current can be in part a result of the broad-scale adjustment of the circulation to an increase in the Changjiang discharge. As a result of this adjustment, the less-saline (CDW) water can be carried to the submerged plateau area between the Changjiang and Cheju Island without any wind forcing.

3.2. Baroclinic Instability of the CDW Plume

[18] The model-predicted summertime CDW plume has a complex salinity and current pattern (Figure 9). After 30 d of Changjiang discharge, the CDW is vertically well-mixed in the shallow area (depth < 20 m) and forms a surface-intensified salinity front or transition zone between the CDW core and the shelf water around the 50-m isobath. This is a typical density front which is baroclinically unstable and creates anticyclonic and cyclonic eddies. With a continuous supply of CDW, anticyclonic eddies grow quickly and extend offshore. In addition to the main southward current, the eddy-induced unstable waves propagate northward at a speed of ~5 cm/s (Figure 11). After 60 d of Changjiang discharge, five well-defined anticyclonic eddies are found at the edge of the front, with accompanying cyclonic eddies (Figure 11). The size of an anticyclonic eddy (measured by the diameter) varies in a range of 30–60 km, which is about three times larger than a cyclonic eddy.

[19] A significant amount of CDW is carried eastward toward Cheju Island as the anticyclonic eddies first elongate and then separate from the CDW plume. This detachment occurs when an opposite current shear forms between each cyclonic eddy and the main body of the CDW plume. This experiment demonstrates that the eastward advection of these detached baroclinic eddies can form the isolated low-salinity lens observed between the Changjiang and Cheju Island.

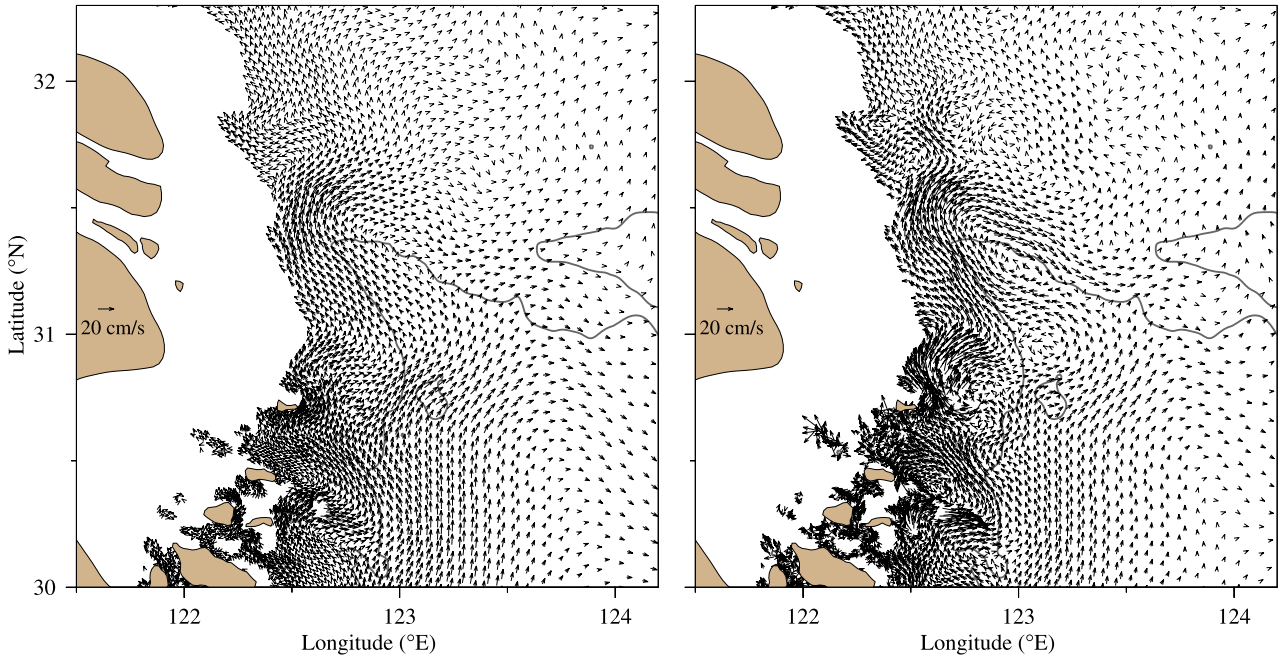

Figure 10. Currents at a depth of 20 m below the surface around the 50-m isobath off the Changjiang at the end of day 30 for the climatology spin-up model run (left) and at the end of day 30 after the Changjiang discharge was added (right). The current vectors were selected in a search radius of ~5 km.

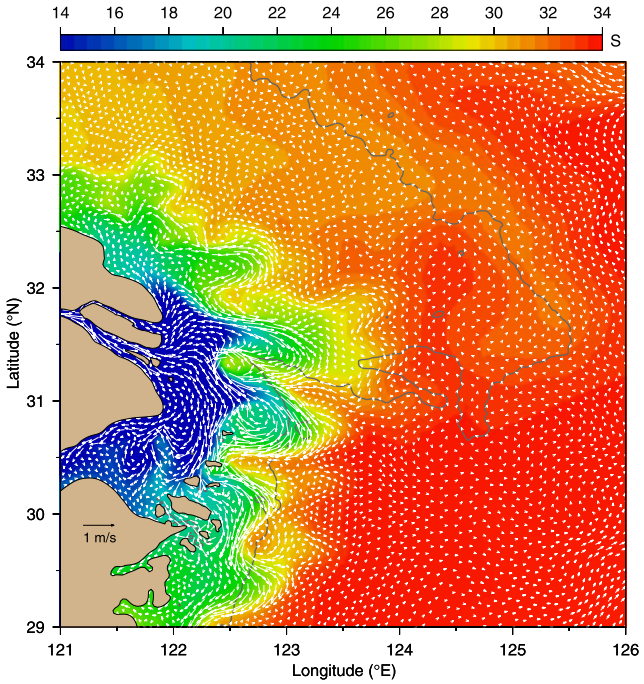

Figure 11. Near-surface CDW plume currents and salinity off the Changjiang at day 60 after the Changjiang discharge was added for the case with only river discharge. The current vectors were drawn with a search radius of ~5 km.

[20] The CDW plume instability found in our numerical experiment is consistent with the previous theoretical study of baroclinic instability of a buoyancy-driven coastal density current by *Qiu et al.* [1988]. They considered an idealized 200-m deep shelf with a straight coastline and found that when the horizontal Ekman number was smaller than a critical value, the density front generated by a sequence of uniformly distributed freshwater sources along the coast became baroclinically unstable. The salinity front first exhibited a wave pattern (with a wavelength of ~100 km in the along-shelf direction) which then evolved into anticyclonic eddies in the wave crests and cyclonic eddies in the wave troughs. The unstable wave crests tended to propagate upstream (in the opposite direction to the main stream of the density current) and low-salinity water was transported to the outer shelf by the detached eddies. In this idealized case, baroclinic instability of the front occurs when

$$E_h = \frac{A_h f}{(g' Q_e)^{2/3}} < E_{hc} \sim 0.34 - 0.57 \qquad (1)$$

where E_h is the horizontal Ekman number, E_{hc} is the critical Ekman number, Q_e is the river discharge per unit length along the coast, A_h is the horizontal eddy viscosity, f is the Coriolis parameter, and g' is the reduced gravity constant.

[21] In our model simulation, CDW flows onto the shelf through multiple passages with an along-shelf extend of ~80 km. With

$$Q_e \sim \frac{60000\,\mathrm{m^3/s}}{8 \times 10^4\,\mathrm{m}},$$

$$f \sim 10^{-4},$$

$$g' = \frac{\rho_2 - \rho_1}{\rho_o} g \sim 0.015 \times 9.8\,\mathrm{m^2/s} = 0.15\,\mathrm{m/s^2},$$

and $A_h \sim 20$ m^2/s given by the Smagorinsky turbulent closure scheme based on the horizontal resolution within the front, the horizontal Ekman number is

$$E_h \sim 0.086 \ll E_{hc}.$$

This indicates that the model Changjiang plume is baroclinically unstable as suggested by *Qiu et al.* [1988].

[22] The model-predicted multiple eddy feature of the CDW plume can be seen in the recent 1-km resolution MODIS (Moderate Resolution Imaging Spectroradiometer) sea surface temperature (SST) image in the ECS/Changjiang received at 1350:26 GMT, 14 September 2005 (Figure 12). This image shows four major outflow passages of CDW and a complex eddy field at the CWD front and in Hangzhou Bay. This observed eddy field is similar in shape and size to that predicted by ECS-FVCOM, supporting the reality of the model-predicted CDW plume in the ECS.

3.3. Effects of Wind Forcing

[23] Wind forcing was added 30 d after initiation of the Changjiang discharge.We ran the model with various wind directions (southerly, southwesterly, southeasterly, westerly, and easterly) and speeds (3, 5, 8, and 10 m/s) typically of those observed during the summer monsoon season in the ECS. A southerly or easterly wind slows the southward along-coast transport in the CDW plume. Owing to the large

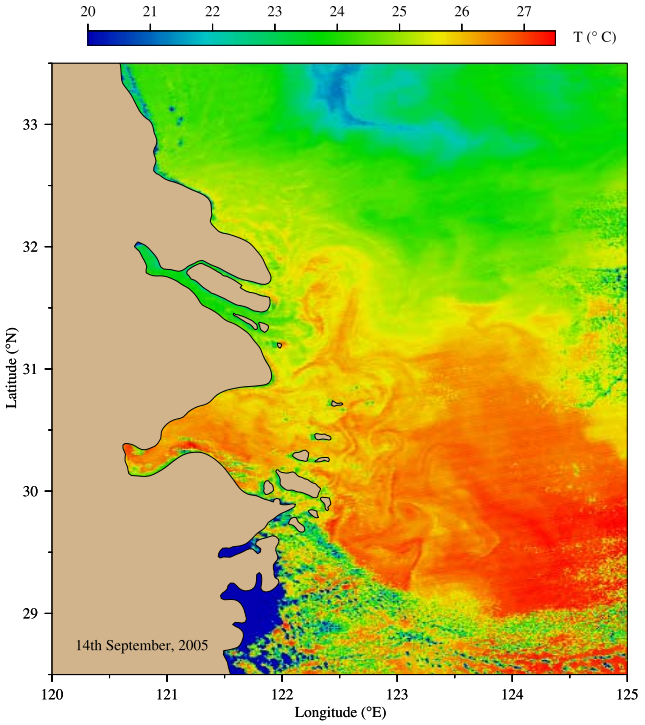

Figure 12. MODIS-derived sea surface temperature image at 1350:26 GMT 14 September 2005 in the western East China Sea area off the Changjiang mouth.

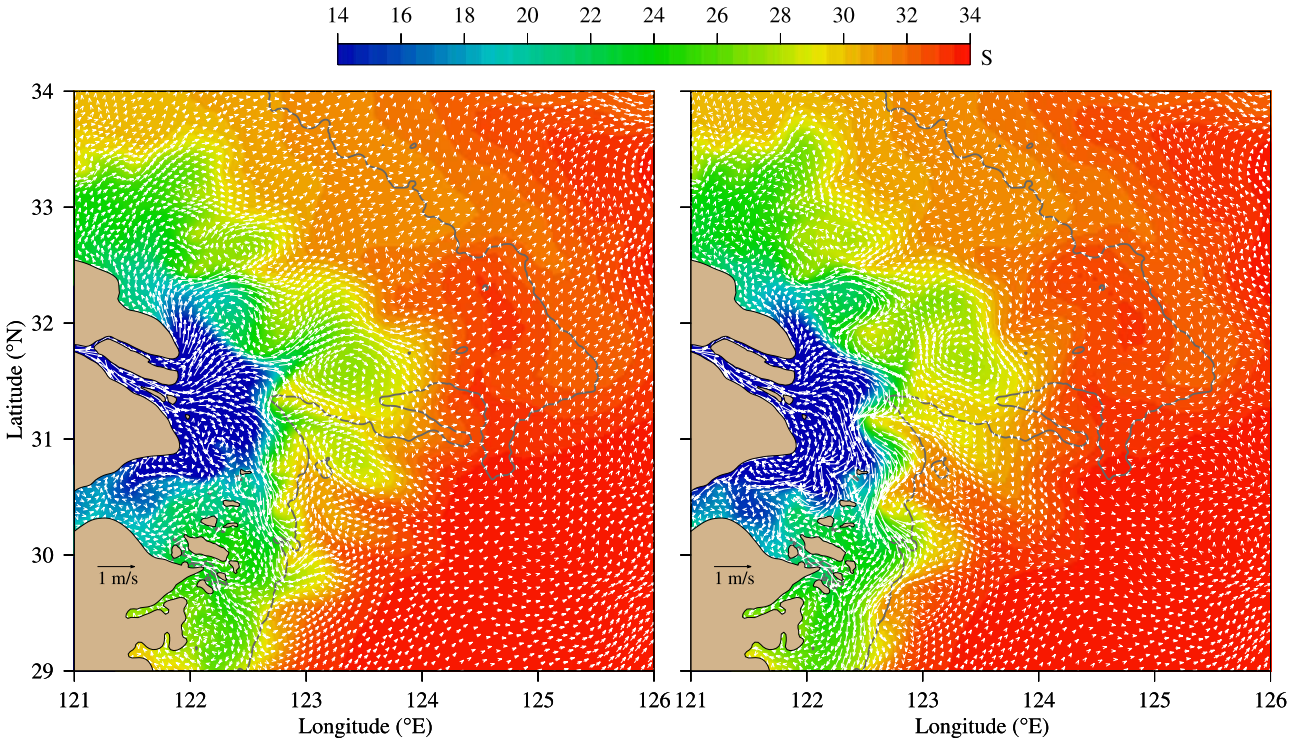

Figure 13. Near-surface CDW plume currents and salinity off the Changjiang on day 30 after a southerly wind of 3 m/s blew (left) and on day 7 after the wind relaxed (right). The wind was added at the end of the 30th day after the Changjiang discharge was added. The wind relaxation (wind speed set to zero) was made at the end of the 30th day after the wind began to blow. Vectors were plotted in the same spatial selection as that shown in Figure 10.

pressure gradient built by the CDW outflow, however, the summer winds have little influence on the CDW current inside the Changjiang. The interaction between wind and CDW plume is strongest near the edge of the salinity front where unstable waves occur. Here the wind tends to speed up and enhance the offshore detachment of CDW. Examples for the southerly wind are described below.

[24] In the case with a constant southerly wind, the wind-induced offshore Ekman transport inside and at front of the CDW off the Changjiang is uniform in space. However, owing to the presence of the frontal waves and eddies, the interaction of wind- and buoyancy-driven currents in the salinity front are spatially nonuniform. For example, in an anticyclonic eddy, the southerly wind intensifies the offshore flow and weakens the onshore flow, increasing an asymmetry of the swirl current and hence speeding up eddy attachment. This is clearly shown seen in the distribution of salinity and currents at day 30 after a southerly wind of 3 m/s is initiated (Figure 13a).

[25] After the wind ceased, the current quickly adjusts to the salinity field and surface elevation within a local inertial timescale. The southward current is restored inside the CDW plume to the prewind condition, while a significant amount of CDW is transported offshore as a result of the offshore detachment of anticyclonic eddies (Figure 13b).

[26] The spatial distribution of CDW varies with wind direction and speed while the interaction process between wind- and buoyancy-driven currents does not change. For the same wind speed of 3 m/s, a southeasterly wind tends to push more CDW northeastward, but the distribution of CDW after the wind ceases is very similar to that found in the case with the southerly wind (Figure 14, left). The southwesterly wind enhances the southeastward transport of CDW and resulting eddy patterns shift southward after the wind relaxation (Figure 14, right). When the southerly wind speed is increased to 5 m/s, the wind-induced Ekman transport causes a larger offshore transport of CDW off the Changjiang. After the wind ceases, less-saline core eddies form east of the Changjiang as a result of the adjustment between the current and salinity fields (Figure 15). Clearly, the stronger southerly wind tends to enhance the offshore transport of CDW as suggested in previous finite-difference model results [*Chang and Isobe*, 2003]. The primary difference here is that in ECS-FVCOM, the offshore transport of CDW is a result of the nonlinear interaction between the wind and unstable eddy fields at the front, while in previous models, the offshore transport is caused by the wind-driven Ekman transport applied to the core body of CDW.

[27] *Chen* [2000] examined the formation of an isolated low-salinity lens and its offshore detachment over the inner shelf of the South Atlantic Bight (SAB). He found that the detachment process happens through two steps. In the first step the spatially nonuniform response of current to the upwelling-favorable wind causes a wavelike frontal shape at the outer edge of the frontal zone. Then the isolated low-salinity lenses form at the crest, when water on the shoreward side of the crest is displaced by relatively high-salinity water advected from the upstream trough south of the crest and diffused upward from deeper off-shelf. The interaction

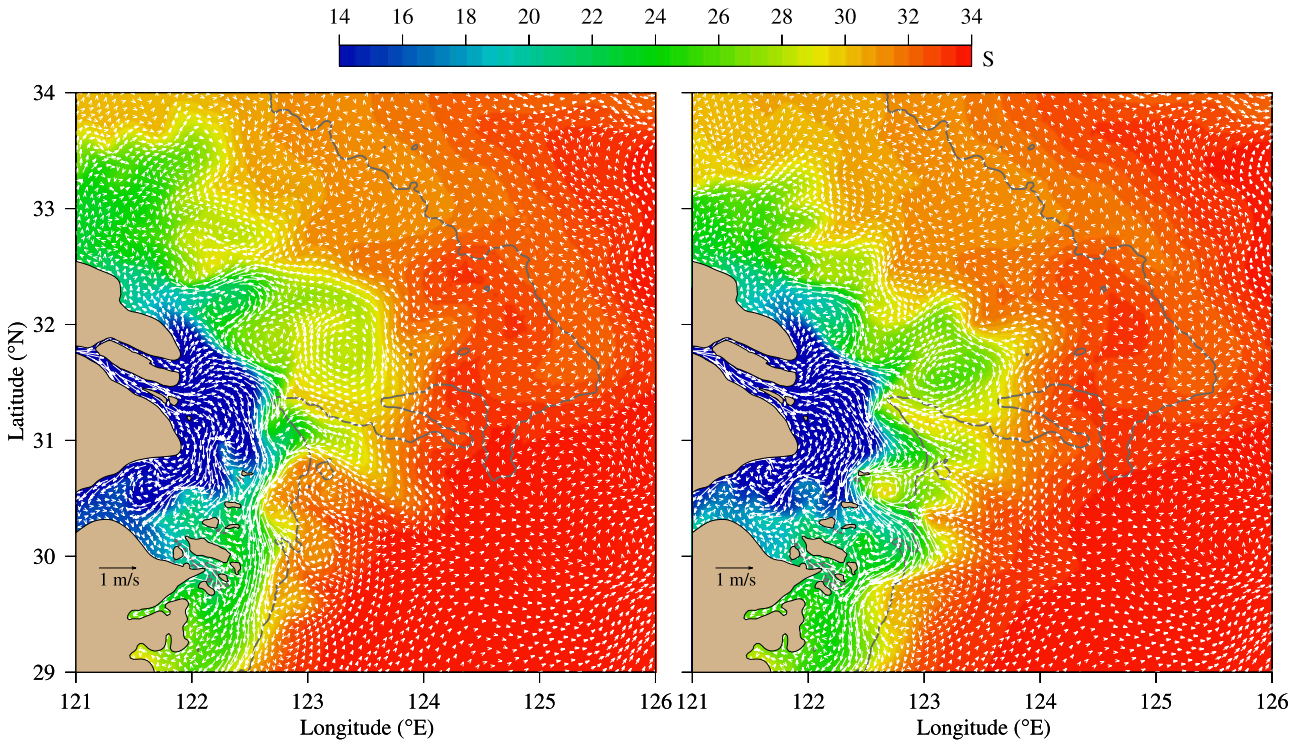

Figure 14. Near-surface CDW plume currents and salinity off the Changjiang on day 7 after the wind relaxed for the cases with southeasterly (left) and southwesterly (right) winds of 3 m/s. The wind ceased at the end of the 30th day after the wind was added. Vectors were plotted in the same spatial selection as that shown in Figure 10.

of wind- and buoyancy-driven currents described here is then similar to the second step found in the SAB, except that the eddy field forms at the CDW front due to baroclinic instability.

[28] Our experiments suggest that when the CDW front becomes unstable, CDW can be transported eastward along the shallow ridge between the Changjiang and Cheju Island as a result of the offshore detachment of anticyclonic eddies. This offshore detachment process can be enhanced significantly by southerly winds, with transport increasing with wind speed. To provide realistic simulation of this offshore transport of CDW, a model needs to resolve the baroclinic instability of the CDW front. This process is missing in previous modeling experiments due to restrictions of horizontal resolution and poor resolution of the "deep" water passages inside and outside of the Changjiang.

3.4. Tracer and Lagrangian Particle Tracking Experiments

[29] To examine the offshore transport of CDW, we conducted both tracer concentration and Lagrangian particle tracking experiments under different physical conditions. Model dye with a concentration of 1.0 was injected throughout the water column on the cross-river mouth transect shown in Figure 16 at the end of 30 model days after initiation of the Changjiang discharge. The dye was then traced for an additional 30 days under conditions with (1) only Changjiang discharge and (2) Changjiang discharge plus a 5 m/s southerly wind, respectively. In the first case, most of the dye appears in the unstable eddy zone along the CDW front and in Hangzhou Bay, while some has been carried eastward of the CDW front along the Changjiang plateau (Figure 16a). In the second case, most of the dye is advected and diffused further offshore to the east and northeast over the Changjiang plateau (Figure 16b). After wind relaxation after 30 d of wind forcing, much of the dye stays over the plateau within the 50-m isobath.

[30] In the particle-tracking experiments, neutrally buoyant particles were released at surface, local middepth, and near-bottom on the same transect as the dye release occurred. On this transect, middepth ranges from 5 to 8 m, and near-bottom depths range from 10 to 16 m. At each level, 50 particles were released uniformly along the transect on the end of 30 d of Changjiang discharge and then tracked for an additional 30 d in the case with only Changjiang discharge and for an additional 60 d in the case with both Changjiang discharge and a 5 m/s southerly wind. In the first case, particles released at the three levels show significantly different trajectories, an indicator of the inhomogeneous flow field in the vertical. The surface particle distribution is similar to the distribution of dye at the surface. The surface particles follow two main paths, one moving offshore toward the CDW front and the other moving southward along the coast and into Hangzhou Bay (Figure 17a). The particles entering the frontal zone move either northward or southward following the complex swirl eddy field. Particles released at middepth also followed two primary paths, one flowing first northward along the coast and then turning clockwise back toward the south in frontal zone and the other directly eastward into the CDW frontal zone (Figure 17b). Some of these particles are ejected from the

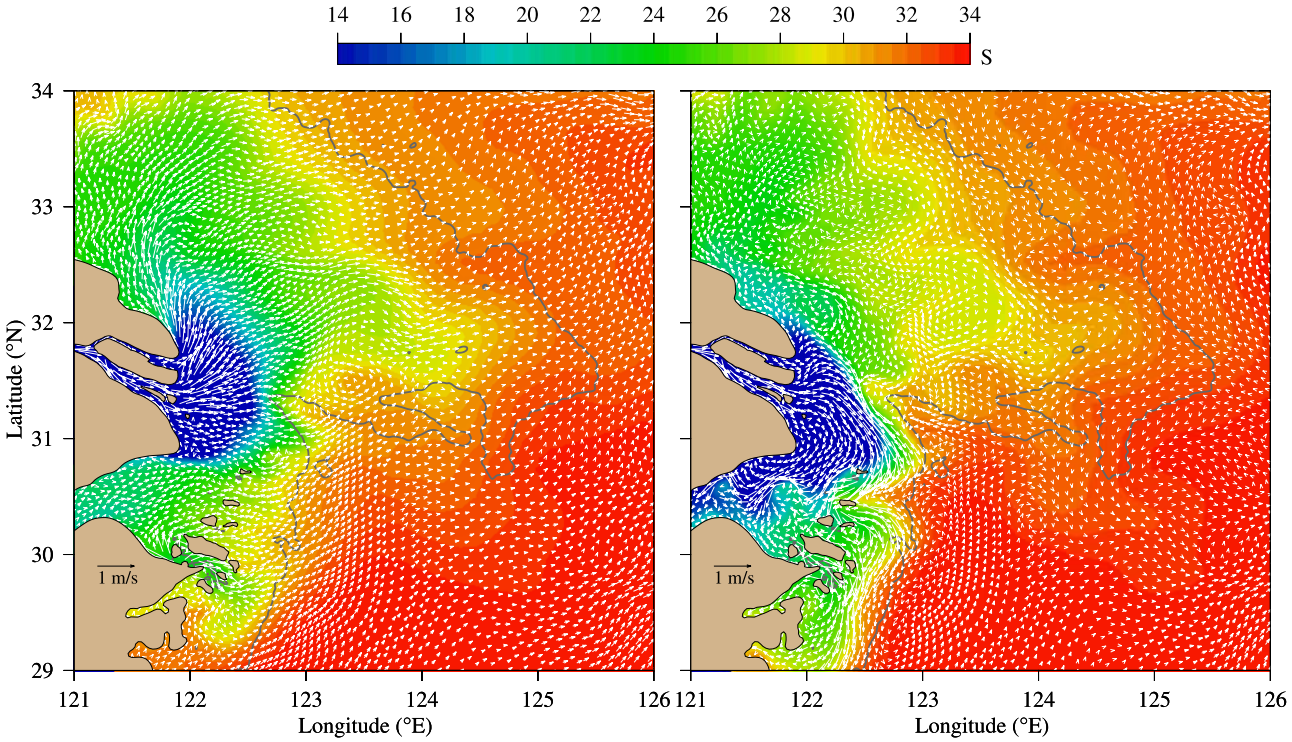

Figure 15. Near-surface CDW plume currents and salinity off the Changjiang on day 30 after a southerly wind of 5 m/s blew (left) and on day 7 after the wind relaxed (right). The wind was added at the end of the 30th day after the Changjiang discharge was added. The wind ceased at the end of the 30th day after the wind blew. Vectors were plotted in the same spatial selection as that shown in Figure 10.

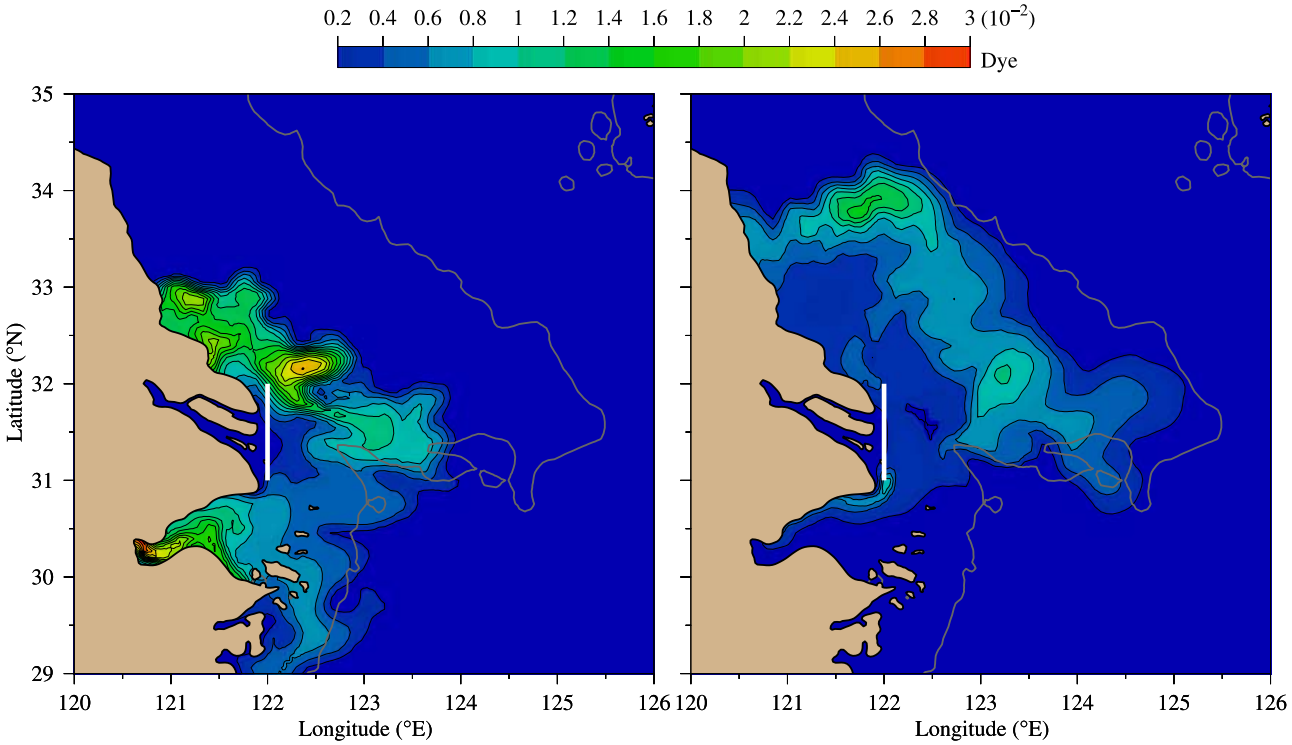

Figure 16. Distributions of model dye concentration at the end of day 60 after the Changjiang discharge was added (left) and at the end of day 7 after the wind relaxed (right). In the wind case, a southerly wind of 5 m/s was added into the model run at the end of day 30 after the Changjiang discharge was started. The wind blew first for 30 days and then set to zero and the model run for an additional 7 d.

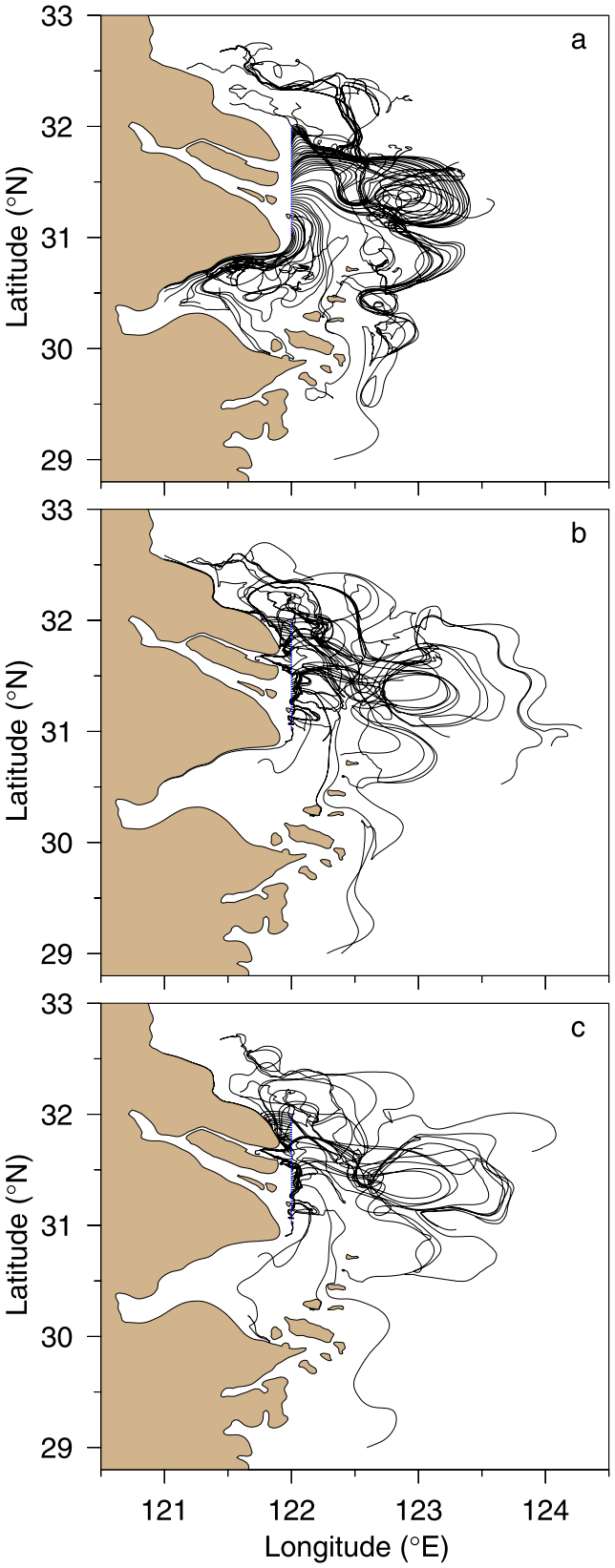

Figure 17. Trajectories of fluid particles released at (a) the surface, (b) local middepth, and (c) near-bottom on the transect off the Changjiang for the case with only Changjiang discharge. The particles were released at the end of day 30 after the Changjiang discharge was added and then traced for additional 30 d.

frontal eddies and move further east and south. Particles released near-bottom follow similar paths as those released at middepth (Figure 17c). Very few particles from these two levels enter Hangzhou Bay.

[31] The particle trajectories differ significantly in the case with a southerly wind of 5 m/s (Figure 18). At the surface, the wind initially causes all surface particles to move eastward offshore in the well-mixed region of the CDW. After these particles enter the CDW frontal zone, some are advected northward along the front while others cross the front on anticyclonic eddy loops and then move eastward toward Cheju Island (Figure 18a). The particles released at middepth show some similarity with the surface particles, with more particles drifting toward Cheju Island (Figure 18b). Even more of the particles released near-bottom escape the frontal zone and move toward Cheju Island (Figure 18c). In this case with a 5 m/s southerly wind, particles take about 40–45 d to travel from the mouth of the Changjiang to Cheju Island. Once entering Cheju Strait, they quickly accelerate and move into the Japan/East Sea through the Tsushima/Korea Strait.

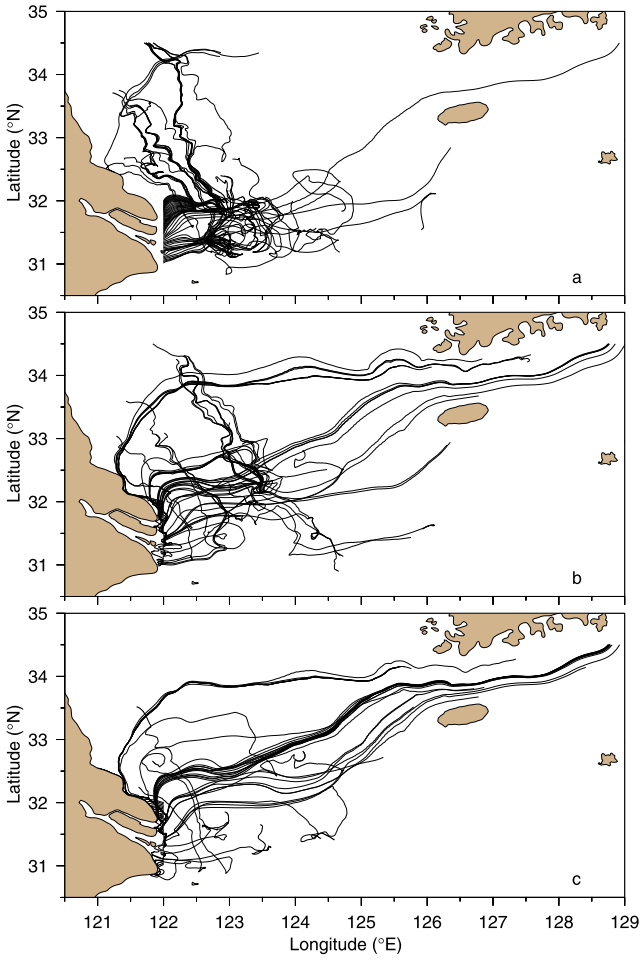

Figure 18. Trajectories of fluid particles released at (a) the surface, (b) local middepth, and (c) near-bottom on the transect off the Changjiang for the case with the Changjiang discharge plus a 5 m/s southerly wind. The particles were released at the end of day 30 after the Changjiang discharge was added and then traced for an additional 60 d.

[32] The model particle trajectories with southerly wind forcing agree the trajectories of drifters observed in September 1986 [*Beardsley et al.*, 1992]. The anticyclonic loop shown in the observed drifter track indicates an anticyclonic eddy at the CDW front, which is well resolved in both our dye and particle experiments using ECS-FVCOM. In particular, the particle-tracking experiments (Figures 18b and 18c) show that a model drifter drogued at 10 m and released off the Changjiang can be carried northeastward into the Cheju Strait and JES as observed in fall 1986.

[33] Note that with a southerly wind, the dye and particles, which were released on the same transect, follow completely different pathways. Dye does not spread to Cheju Strait while many particles arrive there in about 40–45 d. *Chen et al.* [2007] examined physical mechanisms for cross-frontal transport of a neutral tracer on Georges Bank. They found that the movement of the center of the dye concentration (or ''patch'') is driven by the ensemble horizontal velocity and the vertical velocity shear-related concentration flux of the dye patch. In an inhomogeneous flow field the movement of the dye patch can differ significantly from trajectories of individual particles. In our case here, it is inappropriate to study the cross-frontal water exchange based on trajectories of a limited number of particles. During summer, circulation in the ECS is quite inhomogeneous in the vertical. In the CDW frontal zone, the current can be considered as a two-layer system: southward flow of CDW and northward flow of TWC water. In the CDW frontal zone, the formation of an anticyclonic eddy in the upper layer is compensated with a cyclonic eddy near the bottom. Fluid particles release in the upper layer mainly represent the advective movement of a water parcel in the Ekman layer with little interaction with the surrounding water, while the dye movement includes both horizontal and vertical diffusion. Caution is needed when interpreting particle trajectories for water exchange in the ECS.

4. Discussion

[34] The high-resolution ECS-FVCOM simulations reveal that the CDW plume is baroclinically unstable and that CDW can be advected offshore as a result of the detachment of anticyclonic eddies that form in the CDW plume frontal zone. The interaction between wind- and buoyancy-driven flows at the front tends to enhance the offshore CDW transport. A momentum balance analysis shows that the CDW currents off the Changjiang are quasi-geostrophic. In both x and y directions the Coriolis term is balanced to first-order by the difference of barotropic (surface elevation) and baroclinic (density) gradient forces (Figures 19 and 20). This quasi-geostrophic condition is still valid when a uniform southerly wind is added and then turned off. Inside the Changjiang, the presence of wind forcing does not change significantly the along-river distribution of surface elevation: highest at the upstream end of the river and downward toward the mouth (Figure 21). Thus the river flow is controlled by the surface elevation gradient force with little influence from wind or the Coriolis force. This surface elevation gradient plays a key role in stabilizing the CDW flow inside the river and near the coast. Off the Changjiang, the Coriolis force becomes important, and the CDW moves with a balance between the surface elevation gradient and Coriolis forces in the vertically well-mixed region and with a balance between the surface elevation gradient, density gradient, and Coriolis forces in the stratified region. Under such a quasi-geostrophic condition, the evolution of unstable waves and formation of eddies in the CWD front satisfy instability theory [*Pedlosky*, 1979; *Qiu et al.*, 1988]. This theory shows that the instability develops through linear and nonlinear stages. The eddy kinetic energy grows exponentially as a result of transfer from potential energy and mean kinetic energy in the linear stage and decreases gradually as the instability saturates in the nonlinear stage. These two processes are clearly evident in an idealized experiment with multiple river discharges made by *Qiu et al.* [1988], which should be also valid for the CDW plume.

[35] Both previous theoretical and current numerical experiments show that the baroclinic instability of the CDW plume occurs for small horizontal Ekman number that is directly proportional to horizontal diffusion and inversely proportional to river discharge rate. This means that the plume is more unstable during the summer flood season than during the winter dry season. Horizontal diffusion in FVCOM is calculated by the Smagorinsky parameterization method defined as

$$A_h = \frac{0.5 C_H \Omega^{\zeta}}{P_r} \sqrt{\left(\frac{\partial u}{\partial x}\right)^2 + 0.5\left(\frac{\partial v}{\partial x} + \frac{\partial u}{\partial y}\right)^2 + \left(\frac{\partial v}{\partial y}\right)^2} \qquad (2)$$

where C_H is a constant parameter and Ω^{ζ} is the area of the individual tracer control element and P_r is the Prandtl number. The value of A_h is thus proportional to the area of the individual tracer control element and the gradient of horizontal velocities: decreasing as the grid size or horizontal velocity gradient becomes smaller. In general, A_h is a function of time and space related to the horizontal current shear and bathymetry. For the high-resolution ECS-FVCOM grid, $A_h \sim 20$ m^2/s in the CDW plume. This value is much smaller than values used in previous ECS model experiments [*Choi*, 1980; *Yanagi and Takahashi*, 1993; *Isobe et al.*, 2002]. In early summer of 1999, a dye experiment was conducted in the frontal zone on the southern flank of Georges Bank to examine cross-frontal water exchange processes. By tracing the dye patch over time, *Houghton* [2002] used a Fickian model and the dye patch spreading to estimate the cross-frontal horizontal diffusion coefficient and obtained a time-averaged value of A_h in a range of 18 ± 4.5 m^2/s. *Chen et al.* [2007] simulated the dye experiment by running FVCOM with different horizontal resolution on Georges Bank and found that the model converged to a value of A_h of $\sim$20 m^2/s when horizontal resolution was $\leq$500 m. Although there has been no in situ measurements made to estimate A_h in the CDW to our knowledge, we believe that its value should be in the same order of magnitude as that inferred in the frontal zone on the southern flank of Georges Bank because of similar frontal dynamics. Similarity of the eddy fields found in the high-resolution MODIS SST imagery and the ECS-FVCOM simulations implies that the order of the horizontal diffusion coefficient estimated by the Smagorinsky method is robust. We encourage direct in situ measurements in the ECS to improve knowledge of horizontal diffusivity.

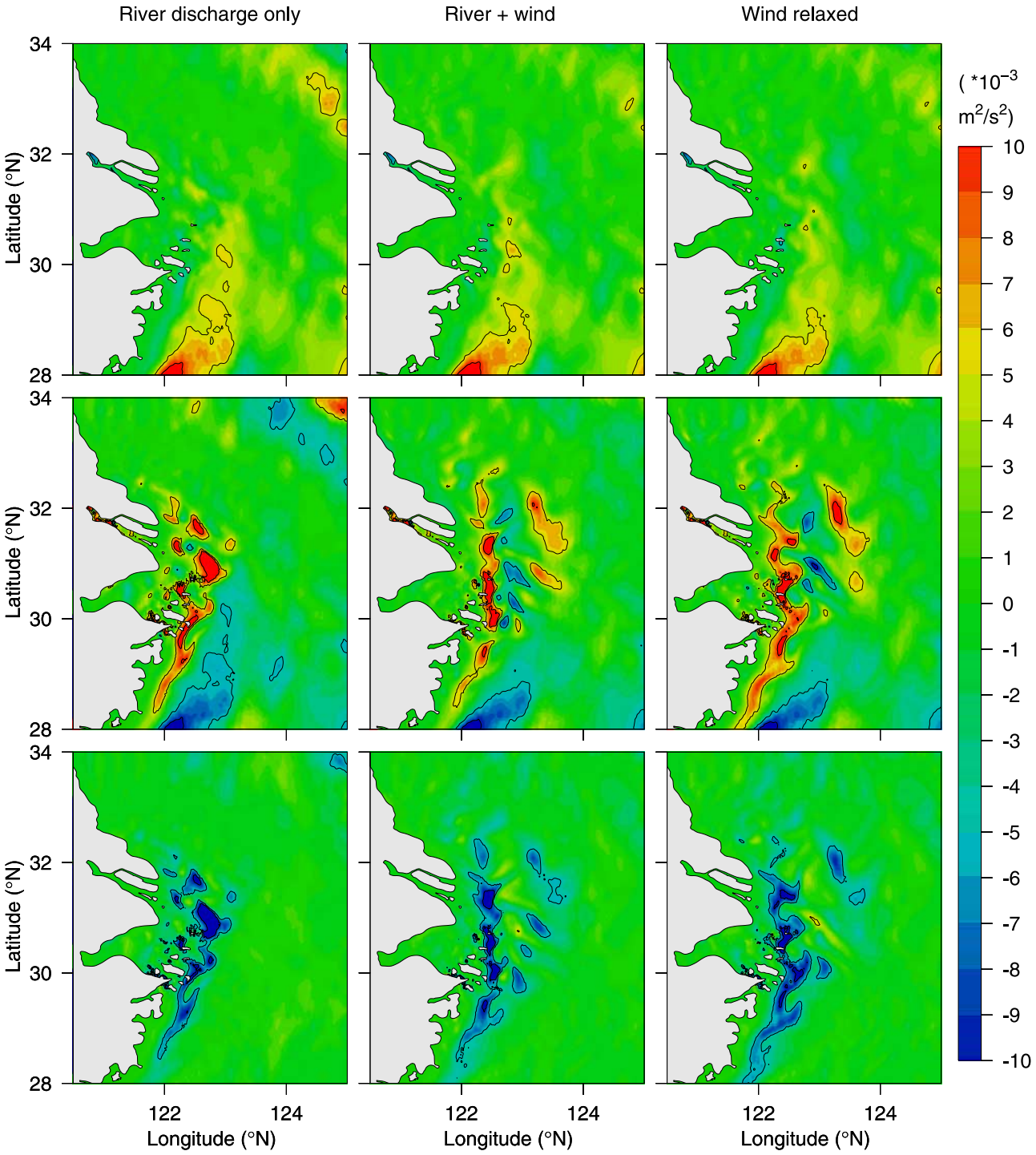

Figure 19. Distributions of the major terms in the vertically averaged *x*-momentum equation on day 60 for the case with only Changjiang discharge (left column), on day 30 after a southerly wind of 3 m/s was added (center column), and on day 7 after the wind relaxed (right column). The top shows the Coriois term, center shows the surface elevation gradient force, and the bottom shows the baroclinic pressure gradient force term. Units are m^2/s^2.

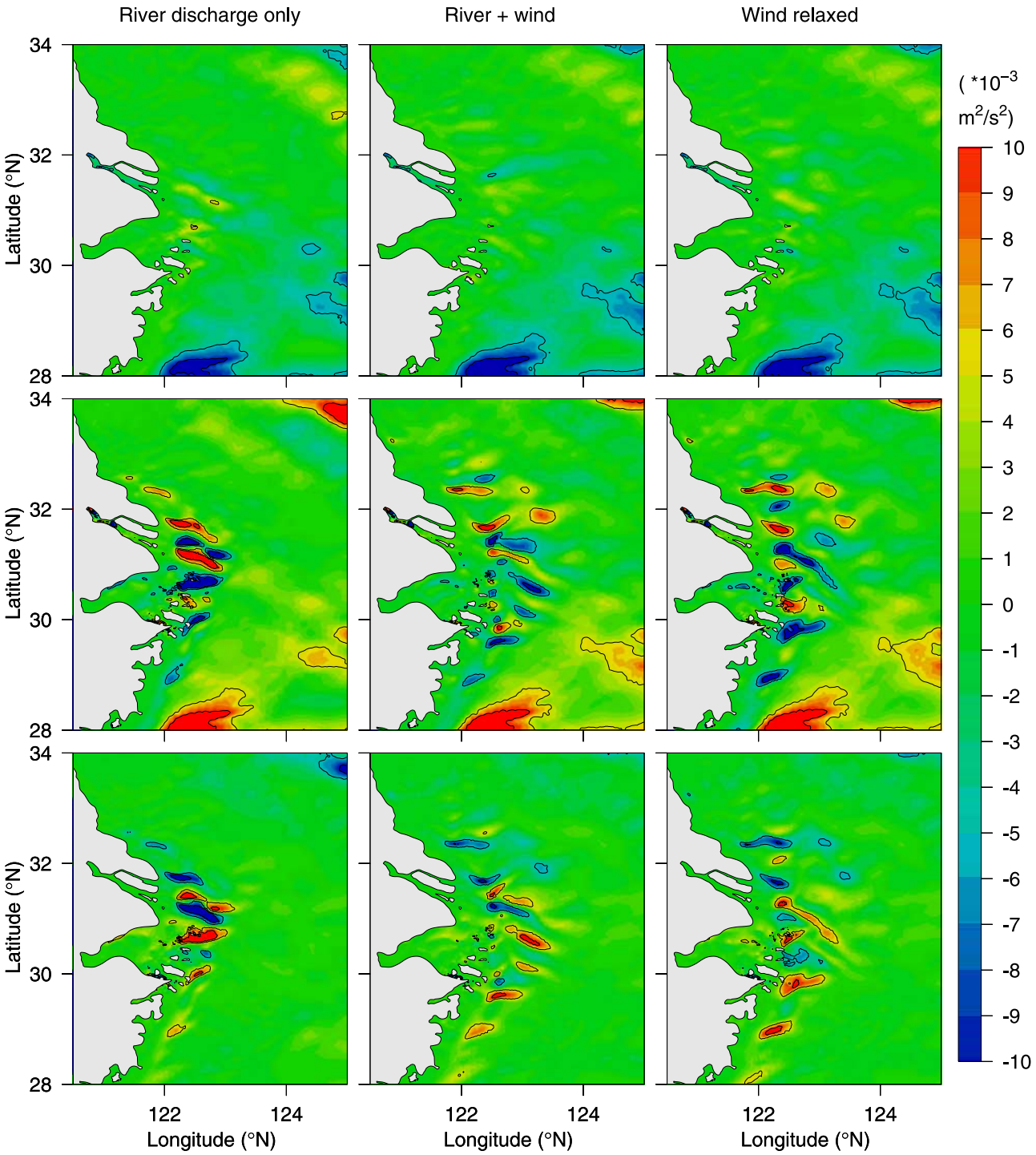

Figure 20. Distributions of the major terms in the vertically averaged *y*-momentum equation (left) on day 60 for the case with only Changjiang discharge, (middle) on day 30 after a southerly wind of 3 m/s was added and (right) on day 7 after the wind relaxed. Also shown is (top) the Coriois term, center panels the surface elevation gradient force and (bottom) the baroclinic pressure gradient force term. Units are m^2/s^2.

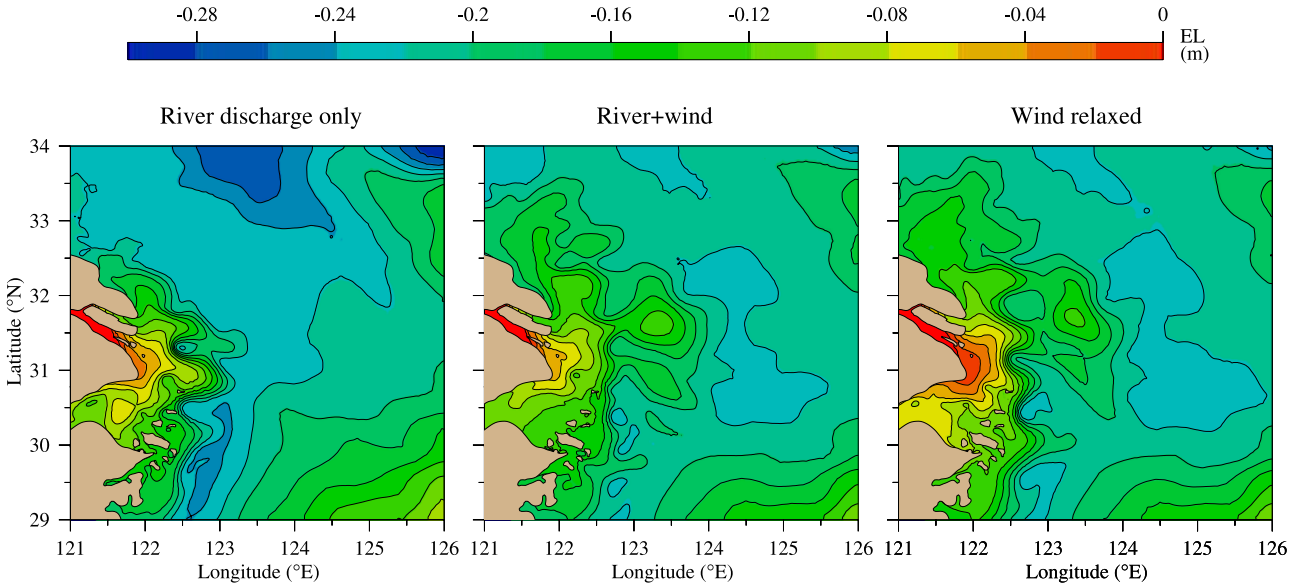

Figure 21. Distribution of the surface elevation (left) at the end of day 60 for the case with only Changjiang discharge, (middle) at the end of day 30 day after a southerly wind of 3 m/s was added, (right) and on day 7 after the wind relaxed.

[36] Our experiments clearly show the advantages of an unstructured grid model in resolving the complex geometry and frontal instability in the ECS. This result is consistent with the other recent application of FVCOM in the ECS by *Isobe and Beardsley* [2006]. By resolving complex bottom topography over the slope, they successfully simulated nonlinear frontal waves and eddies produced by the interaction of Kuroshio with the spatially varying bottom topography. Since the ECS circulation is strongly influenced by the Changjiang discharge and the offshore detachment of CDW is relevant to the baroclinic instability of the CDW front and eddy formation, an numerical mass-conservative unstructured-grid model with geometry flexibility is highly recommended in that region.

[37] ECS-FVCOM is also configured with a higher horizontal resolution Changjiang Estuary subdomain. This subdomain (with a resolution of 0.1∼0.5 km) resolves all major islands off Hanghzhou Bay and the narrow water passages in the Changjiang. This subdomain model can be driven through the grid-nesting approach from the regional ECS-FVCOM. We ran the subdomain model to check whether the horizontal resolution used in the regional model is sufficient to resolve the spatial structure of the Changjiang plume in the inner shelf and also examine the contribution of tidal forcing to the plume instability. We found little difference in the plume structure and behavior, so in this paper we present only the regional ECS-FVCOM model results with a horizontal resolution of ∼0.5 km in the Changjiang. The fine-grid Changjiang subdomain model results have been compared with recent field measurement data and the results will be presented in a separate paper.

5. Summary

[38] Physical processes that cause offshore detachment of CDW into the ECS have been examined using the high-resolution, unstructured-grid, finite-volume coastal ocean model (FVCOM). The numerical experiments show that the summertime ECS regional circulation is strongly influenced by the Changjiang discharge. As a result of the large-scale adjustment, the TWC, YCCC, YCWC, and Tsushima Warm Current are intensified. Low-salinity CDW can be carried eastward over the submerged plateau bounded by the 50-m isobath by either enhanced clockwise vorticity motion of TWC or intensified southeastward transport of YCCC.

[39] Given the horizontal resolution of less than 1.0 km, the CDW front is baroclinically unstable, and CDW can be transported eastward toward Cheju Island by the eddies that detach from the front. This detachment process is enhanced by southerly winds due to the spatially nonuniform interaction of wind-induced Ekman flow and frontal eddy formation and detachment. Characteristics of the model-predicted eddy field are consistent with previous theoretical studies of the baroclinic instability of buoyancy-driven coastal currents and high-resolution MODIS SST imagery for the CDW area taken in the summer of 2005. The baroclinic instability of the CDW front is controlled by the horizontal Ekman number. For the Changjiang, this number is much smaller than the criterion suggested by theoretical analysis.

[40] The model particles show similar trajectories as drifters released off the Changjiang during the summer of 1986. The comparison between these particle trajectories and dye released at the same location suggests that with southerly winds the near-surface particles can be advected to Cheju Island and then enter the JES over a time scale of 40−45 d while the dye spreads more slowly eastward and is still confined to the submerged plateau. Both horizontal and vertical diffusive processes need to be taken into account in order to accurately simulate offshore CDW transport.

[41] We note here that our experiments have focused on an idealized process-oriented study to explore the physical mechanisms for the offshore transport of CDW in the ECS.

More realistic simulations should be carried out to validate the model through comparisons with direct in situ and satellite observations. Since the instability of the CDW front is closely related to local bathymetry and the multiple discharge sources of CDW in the Changjiang mouth, we strongly recommend using an unstructured-grid model with local mass, momentum, and tracer conservation for future studies of coastal processes in the ECS.

[42] **Acknowledgments.** The development of FVCOM is supported by the Massachusetts Fisheries Institute through NOAA grants DOC/NOAA/NA04NMF4720332 and DOC/NOAA/NA05NMF4721131 and also the U.S. GLOBEC Northwest Atlantic/Georges Bank program through NSF grants OCE-0234545 and OCE-0227679, NOAA grant NA160P2323 and ONR subcontract grant from Woods Hole Oceanographic Institution. C. Chen serves as Zi Jiang Scholar at the State Key Laboratory for Estuarine and Coastal Research, East China Normal University. P. Ding is supported by the Chinese National Key Basic Research Project grant 2002CB412403. X. Mao is supported by the National Natural Science Foundation of China (NSFC) grant 40576079. This paper is 07-0201 in the SMAST Contribution Series, School of Marine Science and Technology, University of Massachusetts-Dartmouth.

References

Beardsley, R., R. Limeburner, H. Yu, and G. A. Cannon (1985), Discharge of the Changjiang (Yangtze River) into the East China Sea, *Cont. Shelf Res.*, *4*, 57–76.

Beardsley, R., R. Limeburner, K. Kim, and J. Candela (1992), Lagrangian flow observations in the East China, Yellow and Japan Sea, *La Mer*, *30*, 297–314.

Chang, P. H., and A. Isobe (2003), A numerical study on the Changjiang diluted water in the Yellow and East China Sea, *J. Geophys. Res.*, *108*(C9), 3299, doi:10.1029/2002JC001749.

Chen, C. (2000), A modeling study of episodic cross-frontal water transports over the inner shelf of the South Atlantic Bight, *J. Phys. Oceanogr.*, *30*, 1722–1742.

Chen, C., R. Beardsley, and R. Limeburner (1992), The structure of the Kuroshio southwest of Kyushu: velocity, transport and potential vorticity fields, *Deep Sea Res.*, *39*(2), 245–268.

Chen, C., R. Beardsley, and R. Limeburner (1994), Comparison of winter and summer hydrographic observations in the Yellow and East China Seas and adjacent Kuroshio during 1986, *Cont. Shelf Res.*, *14*, 909–929.

Chen, C., L. Zheng, and J. Blanton (1999), Physical processes controlling the formation, evolution, and perturbation of the low-salinity front in the inner shelf off the southeastern U.S.: A modeling study, *J. Geophys. Res.*, *104*, 1259–1288.

Chen, C., H. Liu, and R. Beardsley (2003), An unstructured grid, finite-volume, three-dimensional, primitive equations ocean model: Application to coastal ocean and estuaries, *J. Atmos. Oceanic Technol.*, *20*(1), 159–186.

Chen, C., G. Cowles, and R. C. Beardsley (2004), An unstructured grid, finite-volume coastal ocean model: FVCOM user manual, 1st ed., *Tech. Rep. 04-0601*, 183 pp., School of Mar. Sci. and Technol., Univ. of Mass., Dartmouth.

Chen, C., R. C. Beardsley, and G. Cowles (2006a), An unstructured grid, finite-volume coastal ocean model (FVCOM) system, *Oceanography*, *19*(1), 78–89.

Chen, C., G. Cowles, and R. C. Beardsley (2006b), An unstructured grid, finite-volume coastal ocean model: FVCOM user manual, 2nd ed., *Tech. Rep. 06-0602*, 315 pp., School of Mar. Sci. and Technol., Univ. of Mass., Dartmouth.

Chen, C., H. Huang, R. C. Beardsley, H. Liu, Q. Xu, and G. Cowles (2006c), A finite-volume numerical approach for coastal ocean circulation studies: Comparisons with finite-difference models, *J. Geophys. Res.*, *112*, C03018, doi:10.1029/2006JC003485.

Chen, C., Q. Xu, R. Houghton, and R. C. Beardsley (2007), A model-dye comparison experiment in the tidal mixing front zone on the southern flank of Georges Bank, *J. Geophys. Res.*, doi:10.1029/2007JC004106, in press.

Choi, B. H. (1980), A tidal model of the Yellow Sea and the Eastern China Sea, *Rep. 80-02*, 72 pp., Korea Ocean Res. and Dev. Inst. (KORDI), Ansan, Korea.

Galperin, B., L. H. Kantha, S. Hassid, and A. Rosati (1988), A quasi-equilibrium turbulent energy model for geophysical flows, *J. Atmos. Sci.*, *45*, 55–62.

He, K. L., P. X. Ding, and Y. Z. Kong (2006), Salinity variation in the southern branch and salt water intrusion in the northern branch of the Changjiang, *Adv. Nature Sci.*, *16*(5), 584–589.

Houghton, R. W. (2002), Diapycnal flow through a tidal front: a dye tracer study on Georges Bank, *J. Mar. Syst.*, *37*, 31–46.

Ichikawa, H., and R. C. Beardsley (2002), The current system in the Yellow and East China Seas, *J. Oceanogr.*, *58*, 77–92.

Isobe, A., and R. C. Beardsley (2006), An estimate of the cross-frontal transport at the shelf break of the East China Sea with the finite-volume coastal ocean model, *J. Geophys. Res.*, *111*, C03012, doi: 10.1029/2005JC003290.

Isobe, A., M. Ando, T. Watanabe, T. Senjyu, S. Sugihara, and A. Manda (2002), Freshwater and temperature transports through the Tsushima-Korea Straits, *J. Geophys. Res.*, *107*(C7), 3065, doi:10.1029/2000JC000702.

Kong, Y. Z., S. L. He, P. X. Ding, and K. L. Hu (2004), Characteristics of temporal and spatial variation of salinity and their indicating significance in the Changjiang estuary, *Acta Oceanol. Sinica*, *26*(4), 9–18.

Lie, H. J., C. H. Cho, J. H. Lee, P. Niiler, and J. H. Hu (1998), Separation of the Kuroshio water and its penetration onto the continental shelf west of Kyushu, *J. Geophys. Res.*, *103*, 2963–2976.

Lie, H. J., C. H. Cho, J. H. Lee, and S. Lee (2003), Structure and eastward extension of the Changjiang River plume in the East China Sea, *J. Geophys. Res.*, *108*(3), 3077, doi: 10.1029/2001JC001194.

Mellor, G. L., and T. Yamada (1982), Development of a turbulence closure model for geophysical fluid problem, *Rev. Geophys.*, *20*, 851–875.

Pedlosky, J. (1979), *Geophysical Fluid Dynamics*, 624 pp. Springer, New York.

Qiu, B., and N. Imasato (1990), A numerical study on the formation of the Kuroshio counter current and the Kuroshio branch current in the East China Sea, *Cont. Shelf Res.*, *10*, 165–184.

Qiu, B., N. Imasato, and T. Waji (1988), Instability of buoyancy-driven coastal density currents, *J. Geophys. Res.*, *93*, 5037–5050.

Smagorinsky, J. (1963), General circulation experiments with the primitive equations, I. The basic experiment, *Mon. Weather Rev.*, *91*, 99–164.

Yanagi, T., and S. Takahashi (1993), Seasonal variation of circulations in the East China Sea and the Yellow Sea, *J. Oceanogr.*, *49*, 503–520.

R. C. Beardsley, Department of Physical Oceanography, Woods Hole Oceanographic Institution, Woods Hole, MA 02543, USA.

C. Chen, G. Cowles, G. Gao, J. Qi, Q. Xu, and P. Xue, Department of Fisheries Oceanography, Intercampus Graduate School for Marine Science and Technology, University of Massachusetts, New Bedford, MA 02744, USA. (c1chen@umassd.edu)

P. Ding, State Key Laboratory for Estuarine and Coastal Research, East China Normal University, Shanghai, 200062, China.

C. Li, Department of Oceanography and Coastal Sciences, School of the Coast and Environment, Louisiana State University, Baton Rouge, LA 70803, USA.

H. Lin, Marine Extension Service, University of Georgia, Athens, GA 30602, USA.

X. Mao, State Key Laboratory of Satellite Ocean Environment Dynamics, Second Institution of Oceanography, State Oceanic Administration, Hangzhou, 310012, China.

M. Shi, College of Physical and Environmental Oceanography, Ocean University of China, Qingdao, 266100, China.